Compounding natural hazards and high vulnerability led to severe impacts from Horn of Africa flooding exacerbated by climate change and Indian Ocean Dipole

Authors

Joyce Kimutai, *Grantham Institute, Imperial College London, UK*
Clair Barnes, *Grantham Institute, Imperial College London, UK*
Mariam Zachariah, *Grantham Institute, Imperial College, London, UK*
Ben Clarke, *Grantham Institute, Imperial College London, UK*
Izidine Pinto, Royal Netherlands Meteorological Institute (KNMI), De Bilt, The Netherlands, Climate System Analysis Group, University of Cape Town, Cape Town, South Africa
Piotr Wolski, Climate System Analysis Group, University of Cape Town, Cape Town, South Africa
Simphiwe Stewart, *Red Cross Red Crescent Climate Centre, the Hague, (based in Johannesburg, South Africa)*
Maja Vahlberg, *Red Cross Red Crescent Climate Centre, the Hague, Netherlands (based in Deärnná/Tärnaby, Sweden)*
Abhinav Banthiya, *Red Cross Red Crescent Climate Centre, the Hague, Netherlands (based in New York, USA)*
Lisa Thalheimer, *United Nations University, Institute for Environment and Human Security, Bonn, Germany*
Friederike E. L Otto, *Grantham Institute, Imperial College London, UK*

Review authors

Dejen Zewdu, *Ethiopian Red Cross Society, Addis Abeba, Ethiopia*
Alebachew Getie, *Ethiopian Red Cross Society, Addis Abeba, Ethiopia*
Julie Arrighi, *Red Cross Red Crescent Climate Centre, the Hague, Netherlands; Global Disaster Preparedness Center, Washington DC, USA; University of Twente, Enschede, The Netherlands (based in New York, USA)*
Malcolm N. Mistry, *Red Cross Red Crescent Climate Centre, the Hague, Netherlands; Environment & Health Modelling (EHM) Lab, Department of Public Health, Environments and Society, The London School of Hygiene & Tropical Medicine (LSHTM), London, UK (based in London, UK)*
Sjoukje Philip, *Royal Netherlands Meteorological Institute (KNMI), De Bilt, The Netherlands*
Sarah Kew, *Royal Netherlands Meteorological Institute (KNMI), De Bilt, The Netherlands*

Main findings

- Historical drought and recent flooding compounded exposure and vulnerability of populations and population sub groups to severity of flood-related impacts
- From the end of October throughout the rainy season up till now rainfall over the region was very heavy, leading to exceptional amounts of precipitation accumulated on several timescales from 1-day to 30-day, with 2023 showing either highest or second highest events on record.
- The October-November-December (OND) rainy season is known to be influenced by modes of natural variability, including the El Niño Southern Oscillation (ENSO) and the Indian Ocean Dipole (IOD) as the dominant modes of variability. Both ENSO and IOD are in a positive phase which has been shown to increase the likelihood of heavy rainfall in the wider Horn of Africa OND season.
- For the region analysed in this study we find no significant role of ENSO but a significant influence of the IOD. In the current IOD phase and under the current climate conditions, an event of this magnitude is expected to happen more often than under IOD neutral conditions, with a return period of approximately 1 in 5. In other words, we would expect to see such an event occurring in every 5th positive IOD-year in the present climate. Overall, taking into account the recent behaviour of the positive IOD, the event would have a return period of around 1 in 40 years in the current climate, that has been warmed by 1.2°C due to the burning of fossil fuels.
- Based on three observation-based data products we find that due to the effect of the IOD, the intensity of the rainfall in the 2023 OND season was about twice what would be expected in a neutral IOD year. Similarly we find that due to the warming of 1.2°C up till now, the magnitude of rainfall has also approximately doubled. Thus, climate change and a positive IOD contributed approximately equally to the magnitude of the event.
- It is important to highlight however that IOD is a natural phenomenon that oscillates between neutral, positive and negative phases while the effect of human-induced climate change will likely continue to increase until the burning of fossil fuels is stopped and emissions reduced to net zero.
- Only very few models exhibit a correlation between the IOD and OND rainfall. These models also show an increase in the intensity attributable to human-induced climate change but smaller than the observations. Combining both observations and models, we estimate that human-induced climate change increased the intensity of OND rainfall by up to a factor of two.
- Due to the low number of models and short observed records we have however low confidence in this quantification, but very high confidence in the overall result that climate change increased the intensity of heavy rainfall in the OND season in the Horn of Africa.
- Longstanding land use land cover (LULC) practices, unsustainable land management in the face of rapid urbanisation, as well as systemic challenges in implementing early warning early action in vulnerable communities increased community-level exposure to extreme rainfall and subsequent flooding.
- Despite existing anticipatory action mechanisms and EWEA (=) protocols, the increasing severity and frequency of extreme weather events in the Horn of Africa (HoA) can potentially overwhelm the operational response capacity of government, development, and humanitarian actors. Ongoing review and reinforcement of response, preparedness, and social protection systems will create a better prepared Horn of Africa.

1 Introduction

The Horn of Africa continues to be heavily impacted by extreme weather and climate-related events (Kilavi et al, 2018; Kimutai et al., 2022; Palmer et at., 2023). Persistent droughts and floods continue to cause hardship for communities and wreck developmental gains. Between late 2020 and early 2023, prolonged drought conditions, exacerbated by anthropogenic climate change (WWA, 2023; Kimutai et al., under review), resulted in widespread impacts to humans, including crop and harvest losses, livestock deaths, hunger, and malnutrition. From late October 2023 onwards, the region experienced flooding associated with heavy rainfall. The enhanced rainfall is currently forecasted to persist into January (KMD, 2023; FEWSNET, 2023). Extensive rainfall in the past few weeks has led to widespread flooding across several Horn of Africa nations, including Ethiopia, Somalia and Kenya. Parts of southern Ethiopia, southern and central Somalia, and eastern Kenya have been mostly impacted with rainfall anomalies of up to 250 mm reported by several weather stations. To date, over three million people have been impacted and close to 300 fatalities have been reported across the three countries (Business Insider, 2023). In Somalia, 110 people have died, and more than one million remain displaced with over 2.4 million people affected in total (OCHA, 2023a). Kenya's death count reached at least 120, with 462.160 people displaced (Business Insider, 2023; Africa News, 2023) by end of November. Ethiopia reported at least 57 fatalities, and over 1.5 million people affected (OCHA, 2023b; OCHA, 2023c). Beyond impacts on humans (fatalities), the Deyr rains have also destroyed key health, transportation, water, sanitation, and electricity infrastructure, as well as schools and businesses across the region. Moreover, it is estimated that 1.5 million hectares of farmland could be destroyed in Somalia alone, whose population heavily relies on agricultural production for livelihoods and is already suffering high rates of acute hunger (IRC, 2023).

Since mid-October, the Somali Red Crescent (SRC) has been committed to alleviating the impacts associated with the heavy rainfall and floods by reinforcing existing programmes across health, WaSH, protection, gender and inclusion, multi-purpose cash, shelter, housing and settlements, livelihoods and basic needs, and more (IFRC, 2023b). Allocated over 611,000 Swiss Francs, local chapters have scaled up their operations, including distributed non-food items including mattresses, blankets, buckets, water purification tablets, and sleeping mats; evacuated residents from high-risk areas; and installed temporary shelters (IFRC, 2023b). Similarly, the Kenyan Red Cross Society (KRCS) was allocated 750,000 Swiss Francs while launching a 18 million Swiss Francs emergency appeal (IFRC, 2023c). As of 23 November, KRCS had provided emergency shelter and essential household items to over 8,500 households; WaSH items to nearly 2,000 households; emergency latrines to 22 camps; health interventions for 3,000 households; and food for nearly 12,500 households (IFRC, 2023c). Moreover, KRCS's Emergency Operations Centre and associated coordination centres are providing first aid and search and rescue operations. Further, the Kenyan government allocated KSh7 billion to implement several programmes to address the impacts of floods. These include airlift medical supplies to enhance rapid response, support for farmers with storage facilities and markets, restore destroyed infrastructure including rehabilitation of dilapidated road networks to facilitate distribution of food and non-food items and delivery of humanitarian assistance to the affected population. Finally, as reported by OCHA (2023), partners in Ethiopia have assisted two million people with food and cash distributions, and 7.1 million people with cholera vaccination. In addition, 510,000 water treatment tablets, 36,000 water purification sachets, 11,000 laundry soaps, and 5,000 body soaps were distributed to over 22,000 affected households. To date,

as of 29 November 2023, the European Commission has mobilised humanitarian funding totaling €3.5 million for affected populations across Kenya, Somalia, and Ethiopia (ECHO, 2023).

The Horn of Africa experiences a bimodal rainfall regime. The main seasons are from March-May 'long rains' and from October-December (OND) 'short rains'. The high seasonal and interannual variability in rainfall experienced in this region result from the complex interaction between local influences, regional circulation patterns, and remote teleconnections. The local factors encompass a diverse range, such as the region's topographic variations, extensive latitudinal span, large inland water bodies, and extensive coastal lowlands. Regional circulation patterns are influenced by processes like Inter-tropical Convergence Zone (ITCZ), Madden-Julian Oscillation (MJO), Quasi-Biennial Oscillation (QBO), and East African Low-Level Jet (EALLJ). Additionally, remote teleconnections come into play, such as the Indian Ocean Dipole (IOD), El Niño Southern Oscillation (ENSO), and variations in the position and strength of subtropical high-pressure cells (including the Mascarene, St. Helena, Azores, and Arabian highs).ENSO and the IOD are known to exert a dominant influence on interannual variability for OND (Indeje et al., 2000, Liebmann et al. 2014). El Niño conditions, which are linked to warmer sea surface temperature (SST) anomalies in the central and eastern Pacific, usually lead to increased rainfall during OND . In contrast, La Niña conditions, characterized by cooler SST anomalies, tend to result in drier OND rains (Uhe et al., 2018). Positive phase of IOD, which is associated with warming of the eastern indian ocean and cooling of the west, is known to enhance El Niño induced precipitation responses and impacts (McLeod, et al., 2020). For instance, the coincidence of the 1997 El Niño with a strong positive IOD event led to extreme wet conditions during OND rainfall season over East Africa. Similarly, the wet conditions in 2019 were associated with the positive phase of IOD. These seasonal short rains were one of the wettest in recent decades (Wainwright, et al., 2020, Palmer et al., 2023). The current El Niño and positive IOD phase are expected to enhance precipitation over the Horn of Africa until 2024 (IRI, Forecast issued November 2023, KMD, 2023; FEWSNET, 2023).

Notably, positive IOD and El Niño conditions have the effect of weakening the Indian Ocean Walker circulation whereby positive SST anomalies in the western Indian Ocean lead to strong rising branch of the Walker circulation, while negative SST anomalies in Southeast Asia result in an anomalous sinking branch of the Walker circulation (Jiang et al., 2021). On the other hand, negative IOD suppresses western arm of the walker circulation, causing drier conditions over the Horn of Africa (Hua et al., 2018; Funk et al., 2018).

1.1 Event definition

In understanding changes in OND rainfall in the Horn of Africa, it is critical to distinguish between signals linked to climate change and those associated with oceanic teleconnections. In this study, we disentangle the role of anthropogenic climate change (i.e., global mean surface temperature; GMST) and IOD in the changes in OND rainfall intensity and the associated return periods. Flood events can arise from short intense events which lead to flash floods or longer events resulting from multi-day accumulations that lead to flooding through saturation of the soil. Therefore to capture a range of possible flood-inducing rainfall processes, we choose two temporal definitions: (i) maximum consecutive 3-day

rainfall (Rx3day) over OND and (ii) maximum consecutive 30-day (Rx30day) rainfall over OND. We compute these indices over a fairly homogeneous region, both in terms of elevation and climatology (refer to Fig. A1 and A2 in the appendix section). The study region is outlined in red in Fig. 1, and hereafter referred to as HoA. The region has distinct long and short rainy seasons and is characterised by arid and semi-arid climate. Additionally, the proposed study domain encompasses the region over which flooding impacts were most experienced.

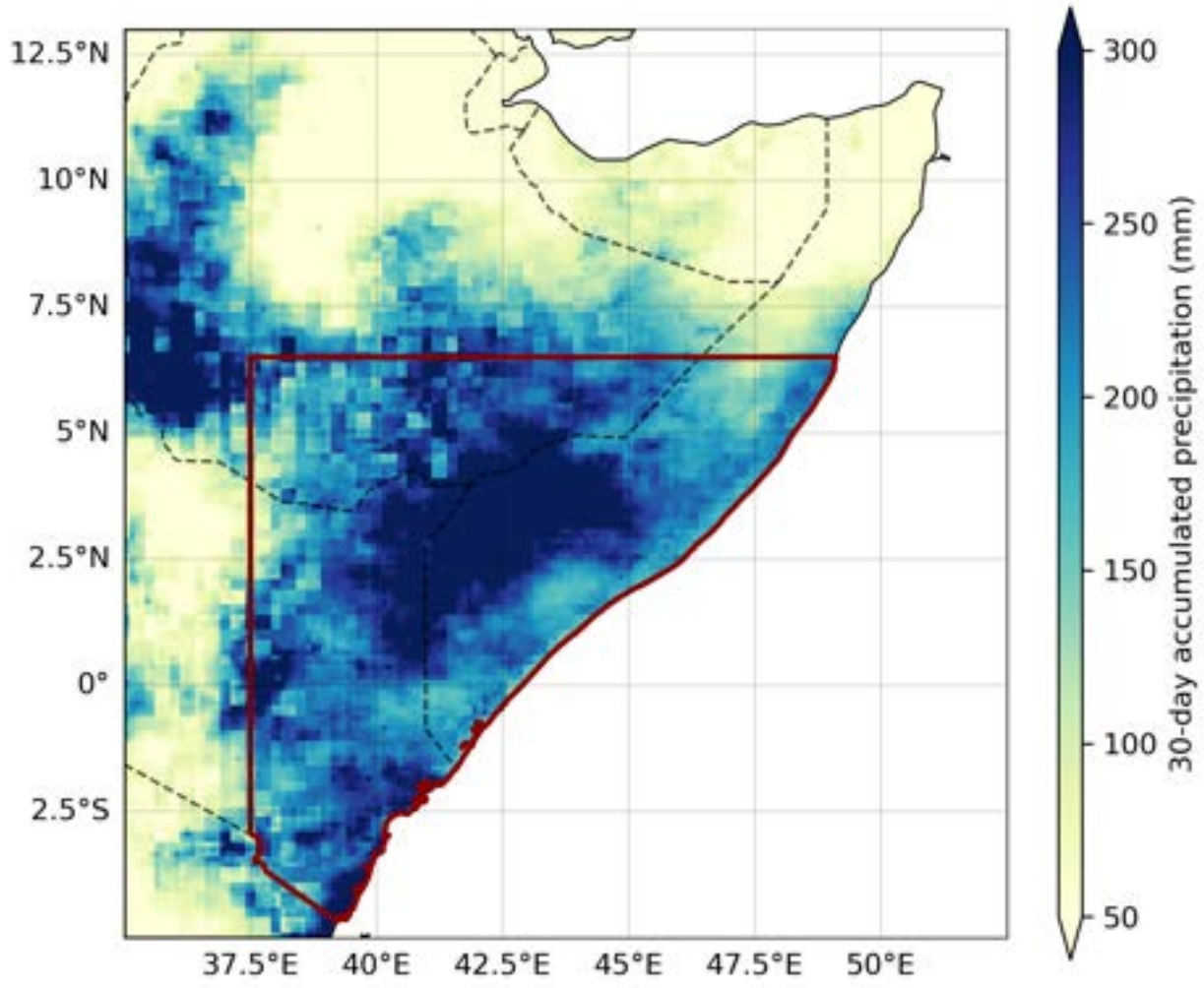

Figure 1. *October- November 30-day rainfall accumulation over the Horn of Africa. Shows the maximum of 30-day cumulative rainfall on the 20th of November 2023 over the region that experienced highest flood-induced impacts. Source: MSWEP data.*

2 Data and methods

2.1 Observational data

We use three gridded observational daily rainfall datasets. (i) Global Unified Gauge-Based Analysis of daily precipitation (CPC) (ii) Multi-Source Weighted-Ensemble Precipitation (MSWEP) (iii) Tropical Applications of Meteorology using SATellite and ground based observations (TAMSAT). Station data is available from Kenya Meteorological Department (KMD) while the gridded products are available as follows. CPC data is the gridded product from NOAA PSL, Boulder, Colorado, USA known as the CPC Global Unified Daily Gridded data, available at 0.5° x 0.5° resolution, for the period 1979-present. Data are available from NOAA. The Multi-Source Weighted-Ensemble Precipitation (MSWEP) v2.8 dataset (updated from Beck et al., 2019) is fully global, available at 3-hourly intervals and at 0.1° spatial resolution, available from 1979 to ~3 hours from real-time. This product combines gauge-, satellite-, and reanalysis-based data. The Climate Hazards Group InfraRed Precipitation with Station data (CHIRPS), a commonly used gridded dataset for the region is only available until the end of October and thus could not be used at the time of undertaking this rapid assessment.

Figures 2-4 show cumulative OND rainfall over the study region for different length of accumulation. The 2023 event is the highest on record for 1, 3 and 5-day accumulation in MSWEP, 3- and 5-day in CPC and combined highest for 30-days in TAMSAT. For all other lengths of cumulative rainfall it is second highest in CPC and MSWEP, but lower in TAMSAT. It is important to highlight that the 2023 accumulation is only including October and November, as December is still ongoing at the time of writing.

MSWEP and CPC show very similar patterns of year to year variability but with different amplitudes. TAMSAT has more wet years at the beginning of the record. All three datasets show similar behaviour to the KMD stations at the end of the timeseries for the 14 available stations in the Kenyan part of the study region. A map of the time series comparison plots can be found in the Annex (Figures A3 and A4).

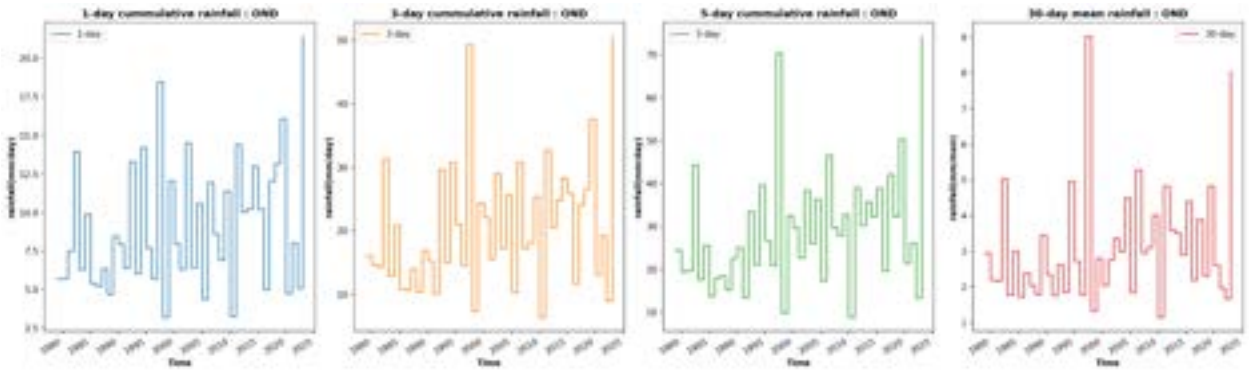

Figure 2. Maximum of *October- December rainfall accumulation over the Horn of Africa for different times of accumulation in MSWEP.*

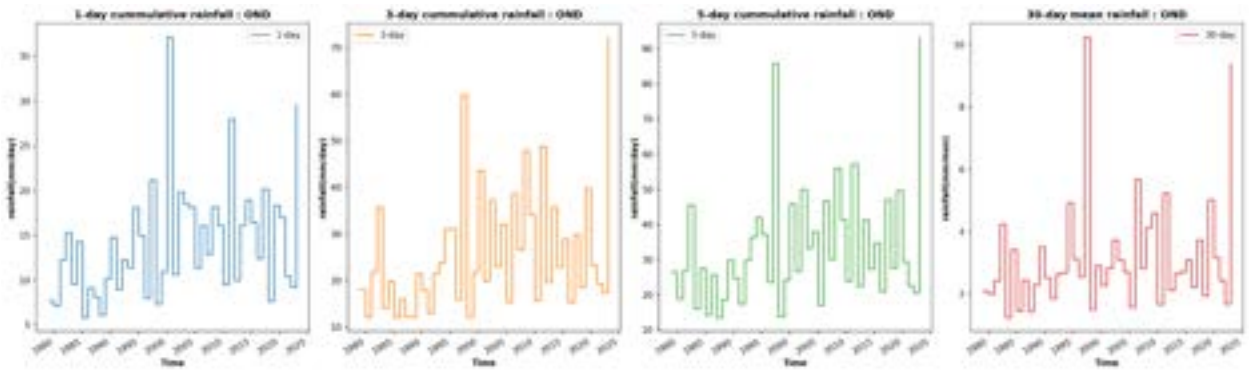

Figure 3. *As figure 2 but for CPC.*

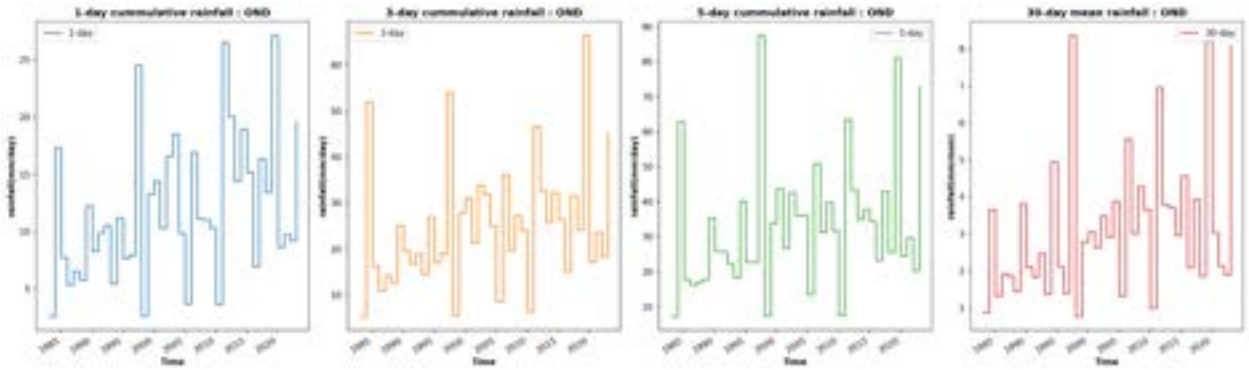

Figure 4. *As figure 2 but for TAMSAT.*

As a measure of anthropogenic climate change we use the (low-pass filtered) 4-year smoothed GMST, where GMST is taken from the National Aeronautics and Space Administration (NASA) Goddard Institute for Space Science (GISS) surface temperature analysis (GISTEMP; Hansen et al., 2010; Lenssen et al. 2019). And as a measure of the ENSO we use the relative Nino3.4 index as defined in Van Oldenborgh et al., 2021. This is the Nino3.4 index (average SST over 5° S–5° N, 120°–170° W) minus the SST between 20° S–20° N to adjust the index for climate change. Because we are averaging the index over a period of several months, the values are not standardised per calendar month.

Time series of the observed IOD and Nino3.4 index are derived from the ERSST dataset and obtained from KNMI's Climate Explorer tool. In the absence of updated values for November and December 2023, the annual mean from September-November was used as the covariate, with the 2023 value based on the September-October mean. The correlation between the SON IOD and Rx30day was found to be comparable to the correlation between OND IOD and Rx30day, so this is not expected to substantively affect the conclusions.

Time series of IOD for the climate models was downloaded from the Climate Variability Diagnostics Package.

2.2 Model and experiment descriptions

We use four multi-model ensembles from climate modelling experiments using very different framings (Philip et al., 2020): Sea Surface temperature (SST) driven global circulation high resolution models, coupled global circulation models and regional climate models.

1. Coordinated Regional Climate Downscaling Experiment (CORDEX)-Africa (0.44° resolution, AFR-44) multi-model ensemble (Nikulin et al., 2012), comprising of 29 simulations resulting from combinations of 12 Global Climate Models (GCMs) and 8 Regional Climate Models (RCMs). These simulations are composed of historical simulations up to 2005, and extended to the year 2100 using the RCP8.5 scenario.

2. Coordinated Regional Climate Downscaling Experiment (CORDEX)-Africa (0.22° resolution, AFR-22) multi-model ensemble (Gutowski et al., 2016; Giorgi et al., 2021), comprising 10 simulations resulting from combinations of 5 GCMs and 4 RCMs. These simulations are composed of historical simulations up to 2005, and extended to the year 2100 using the RCP8.5 scenario.

3. HighResMIP SST-forced model ensemble (Haarsma et al. 2016), the 11 simulations of which span from 1950 to 2050. The SST and sea ice forcings for the period 1950-2014 are obtained from the 0.25° x 0.25° Hadley Centre Global Sea Ice and Sea Surface Temperature dataset that have undergone area-weighted regridding to match the climate model resolution (see Table B). For the 'future' time period (2015-2050), SST/sea-ice data are derived from RCP8.5 (CMIP5) data, and combined with greenhouse gas forcings from SSP5-8.5 (CMIP6) simulations (see Section 3.3 of Haarsma et al. 2016 for further details).

4. CMIP6. This consists of simulations from several models with varying resolutions. For more details on CMIP6, please see Eyring et al., (2016). For all simulations, the period 1850 to 2015 is based on historical simulations, while the SSP5-8.5 scenario is used for the remainder of the 21st century.

2.3 Statistical methods

In this report, we analyse time series of annual maxima of 3-day and 30-day accumulated precipitation over the region outlined in figure 1 during the short rains (October-November-December), henceforth referred to as RX3day and RX30day respectively. The analysis steps include: (i) trend calculation from observations; (ii) model evaluation; (iii) multi-method multi-model attribution and (iv) synthesis of the attribution statement. In order to compare the present climate and the climate of the past, defined respectively by the GMST values of 2023 and of a 1.2°C cooler climate representing the preindustrial past (1850-1900, based on the Global Warming Index) we use a nonstationary Generalised Extreme Value (GEV) distribution that scales with both GMST and the IOD as explained below (sec. 2.3.1). We use this model to estimate the return period of the event, along with the probability ratio (PR; the factor-change in

the event's probability) and change in intensity of the 2023 event. Results from observations and models that pass the evaluation tests are synthesised into a single attribution statement.

Methods for model evaluation and synthesis are used according to the World Weather Attribution Protocol, described in Philip et al. (2020), with supporting details found in van Oldenborgh et al. (2021), Ciavarella et al. (2021) and here. The method used in observational and model analysis is modified from the standard method outlined in the protocol to accommodate trends dependent on both GMST and the IOD, as described in detail below. A similar approach was also used to examine the effects of ENSO on low precipitation in the same region in Kimutai et al. (2023).

2.3.1 Statistical modelling of the combined effect of GMST and IOD

As discussed in Section 1, the OND rainy season in eastern Africa is known to be influenced by natural modes of variability, particularly the IOD and theENSO. Rainfall totals during periods of both positive ENSO and positive IOD can be 2 to 3 times more than the average of OND season (Wainwright, et al., 2020); however, given that this is a rapid study, we do not attempt to disentangle the effects of ENSO and IOD on precipitation, but focus on the effect of the IOD, which is considered to have the stronger impact of the two oscillations on OND rainfall (e.g., Behera et. al., 2005, Liebmann et al. 2014, MacLeod, et. al., 2021). Future work is needed to identify whether ENSO, even though it was not found to significantly affect OND rainfall on its own in initial tests, affects rainfall in combination with IOD.

In order to examine the effect of the IOD on RX3day and RX30day alongside that of increasing GMST, we extend the nonstationary model to accommodate an additional covariate. The variable of interest, X, is assumed to follow a GEV distribution in which the location and scale parameters vary with both GMST and IOD:

$$X \sim GEV(\mu, \sigma, \xi \mid \mu_0, \sigma_0, \alpha, \beta, T, D),$$

where X denotes the variable of interest, RX3day or RX30day; T is the smoothed GMST, D is the IOD index, μ_0 and σ_0 are the mean and variance parameters of the nonstationary distribution and α, β are the trends due to GMST and the IOD, respectively. As a result, the location and scale of the distribution have a different value in each year, determined by both the GMST and IOD. Maximum likelihood estimation is used to estimate the model parameters, with

$$\mu = \mu_0 exp\left(\frac{\alpha T + \beta D}{\mu_o}\right) \quad \text{and} \quad \sigma = \sigma_0 exp\left(\frac{\alpha T + \beta D}{\mu_o}\right).$$

This formulation reflects the Clausius Clapeyron relation, which implies that precipitation scale exponentially with temperature (Trenberth et.al., 2003, O'Gorman and Schneider 2009). Throughout this study, the distribution is evaluated with IOD index D fixed at the 2023 value in both the current and 1.2°C cooler climate distributions, in order to obtain the change in intensity of the extreme 2023 OND rainfall event due to climate change. Under this model, the effects of GMST and the IOD are assumed to be independent of one another, so that the change in intensity due to GMST is unaffected by the change in intensity due to the IOD.

2.3.2 Estimation of return periods

Extra care must be taken when reporting and interpreting return periods that depend on more than one covariate. Typically, WWA reports estimated return periods for the event of interest under current climatic conditions: that is, with the GMST fixed at the 2023 level. In this study, there are two covariates to consider: the GMST and IOD. By fixing both the IOD and the GMST at their 2023 levels, we can estimate the return period of the 2023 event in the current climate and in the current IOD state. Mathematically, this return period is written as

$$1 / P(X > x_{2023} \mid T = t_{2023}, D = d_{2023}),$$

where x_{2023} is the 2023 value of observed precipitation; t_{2023} denotes the 2023 GMST; and d_{2023} denotes the 2023 IOD. Altogether, the expression in brackets gives the probability that X will exceed x_{2023}, given that $T = t_{2023}$ and $D = d_{2023}$; inverting this probability gives us an expected return time, in years.

However, this return period only tells us the probability of experiencing a similar event under current IOD conditions. In order to understand how frequently such an event is actually likely to occur, we must account for the fact that the IOD is not often in the strongly positive phase observed in 2023. To do this, we evaluate the return period over all states of the IOD that have been recorded since 1980 (the period covered by the available gridded data products). This is done by first averaging the probability of exceeding x_{2023} over all recorded values of d_{2023}, then inverting to obtain the return period:

$$1 / \sum_{y=1980}^{2023} P(X > x_{2023} \mid T = t_{2023}, D = d_y).$$

3 Observational analysis: return period and trend

In Section 1, event definitions of 3-day and 30-day accumulated precipitation were considered, in order to reflect the different timescales at which impacts were reported. However, qualitatively similar results to those presented here were obtained when the analysis was carried out using RX3day, and so we only discuss the RX30day analysis in detail here. The results of the observational analysis of RX3day are shown in the Appendix (Figures A5-A8).

Here we present the results of fitting the nonstationary GEV described in Section 2.3.1 to the time series of RX30day derived from the MSWEP, TAMSAT and CPC datasets, using GMST and IOD as covariates.

Figure 3 shows the time series of RX30day in each dataset, with the fitted model overlaid. The time series are fairly similar, although TAMSAT is slightly more variable than both CPC and MSWEP in recent decades; we therefore retain all three observational datasets in the attribution analysis. The fitted trend over time is highly variable, reflecting the strong influence of the IOD on the expected precipitation, but generally captures the peaks of the observed rainfall well.

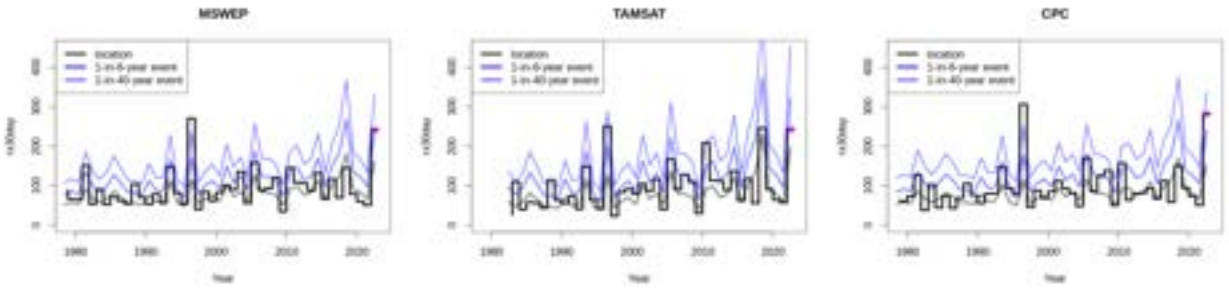

Figure 5: *Time series of RX30day over the study region in the MSWEP, TAMSAT and CPC datasets. The pink dot marks the 2023 event; the heavy black line indicates the location of the fitted distribution, and the blue lines indicate estimated 6- and 40-year return levels.*

The contributions of the GMST and IOD to the fitted model can be seen in Figures 4 and 5. Figure 4 shows the observed values of RX30day in all three datasets, plotted against the IOD; the fitted model shows the location of the fitted distribution in the 2023 climate, while the blue lines show the expected return levels of 6-year and 40-year events. There is a clear relationship between the IOD and RX30day, with the heaviest precipitation always associated with very high values of the IOD; in the current climate, the 2023 event is unusual but not very extreme when the strength of the current IOD phase is taken into account, falling below the 40-year threshold in all three datasets. According to the model fitted to the MSWEP dataset, the precipitation was made 90% more intense due to the strongly positive phase of the IOD (95% confidence interval: 45-186); in TAMSAT, 143% more intense (63-289%); and in CPC, 83% more intense (12-183%). Although the uncertainties on these estimates are very wide, they do not span zero, and we can therefore be confident that the heavy precipitation was made substantially more intense by the strongly positive phase of the IOD: roughly double what it would have been if the IOD had been in a neutral phase.

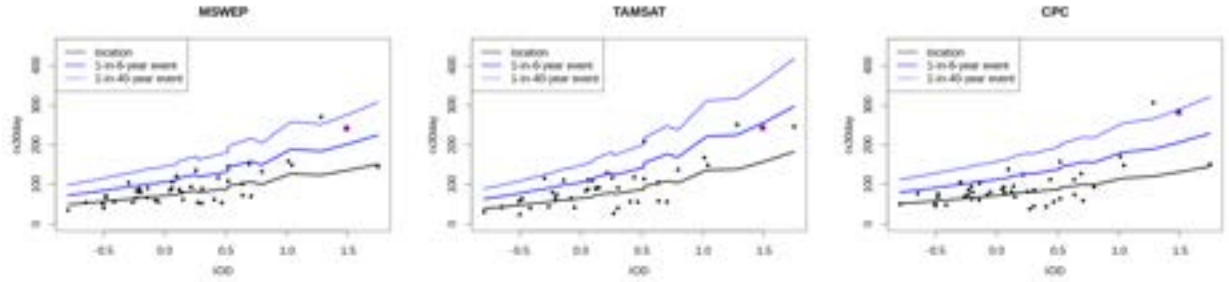

Figure 6: *Observed values of RX30day in the MSWEP, TAMSAT and CPC datasets, plotted against the IOD, with the GMST held fixed at the 2023 level. The pink dot marks the 2023 event; the heavy black line indicates the location of the fitted distribution, and the blue lines indicate estimated 6- and 40-year return levels.*

Figure 5 shows RX30day and the same fitted models, now plotted against GMST, showing the location and expected return levels when the IOD is in a neutral phase (i.e. IOD = 0). Several points fall far above the expected 40-year return level; this is because much of the variability in these time series - particularly in the wettest years - is explained by the IOD and not by the GMST. However, there is evidence of an overall increasing trend in RX30day as temperatures warm. According to the model fitted to the MSWEP dataset, the precipitation was made 87% more intense due to climate change (95% confidence interval:

34-129); in TAMSAT, 128% more intense (49-202%); and in CPC, 71% more intense (14-128%). Although the uncertainties on these estimates are very wide, they again do not span zero; we can therefore also be confident that the heavy precipitation was also made substantially more intense by increased GMST, with the 2023 event roughly twice as intense as it would have been in a preindustrial climate. Overall, the strongly positive IOD phase this year increased the intensity of the event by roughly the same amount.

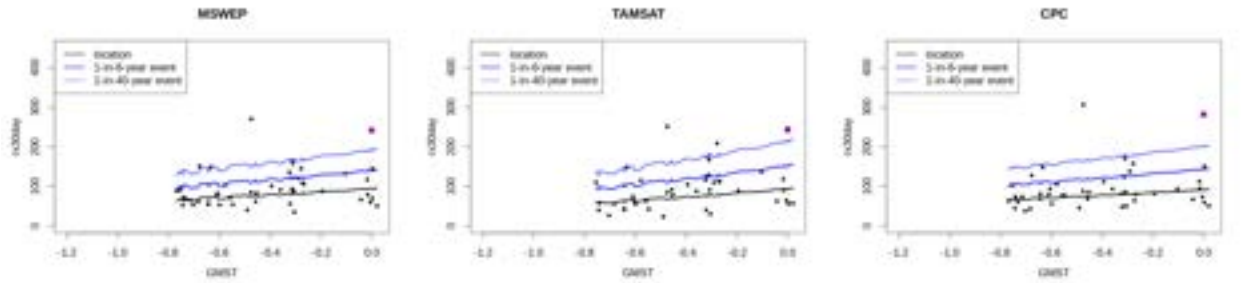

Figure 7: *Observed values of RX30day in the MSWEP, TAMSAT and CPC datasets, plotted against GMST, with the IOD held fixed at 0. The pink dot marks the 2023 event; the heavy black line indicates the location of the fitted distribution, and the blue lines indicate estimated 6- and 40-year return levels.*

Figure 6 shows the estimated effective return levels of the observed RX30day, transformed to the 2023 climate (in red) and to a cooler climate (in blue), still in the strong positive IOD phase recorded in 2023. In all three datasets, the model fits the data fairly well, with the exception of the heaviest precipitation events, which tend to be higher than the model predicts: this may be due to an interaction between GMST and the IOD, or between ENSO and the IOD, that is not captured in the model.

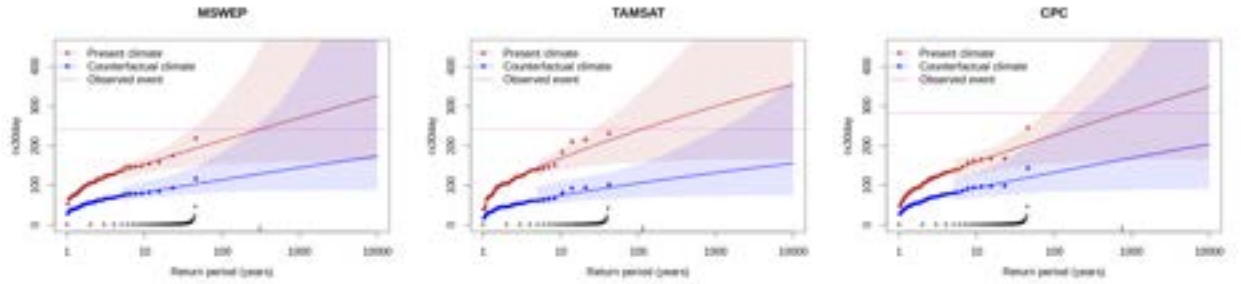

Figure 8: *Expected return levels of RX30day for the 2023 climate (red lines) and a hypothetical 1.2C cooler climate (blue lines) in the current strongly positive phase of the IOD. Shaded regions indicate 95% confidence intervals.*

According to the model fitted to the MSWEP dataset, events of similar magnitude to the 2023 event are expected to occur once in every 6 years with a strongly positive IOD phase (95% confidence interval: 1-150); in TAMSAT, once every 2 years with strongly positive IOD (1-14); and in CPC, once every 13 years with strongly positive IOD (2-10236). Taking these results together, we estimate that events of comparable magnitude might be expected to occur once every five years in which the IOD is in a strongly positive phase.

Taking into account the range of IOD states observed since 1980 following the method outlined in Section 2.3.2, events of similar magnitude to the 2023 event are expected to occur once every 53 years overall according to MSWEP (95% confidence interval: 13-1400); once every 20 years according to TAMSAT

(8-120); and once every 120 years according to CPC (20-infinite). Based on these results, we use a return period of 40 years for this event for the remainder of this study.

Due to the large uncertainties in the return period of the event, we do not report probability ratios for this event, and will focus instead on the change in intensity. We use the same statistical model - including both GMST and IOD as covariates - for the model analysis, and Section 6 presents a synthesis of the results of this analysis.

4 Model evaluation

Climate models are evaluated first for their ability to capture the observed relationship between IOD and RX30day prior to 2023. The Pearson correlation between the observed RX30day time series and the September-November IOD was computed for each of the three observational datasets, along with a bootstrapped 95% confidence interval. The same correlation was then also computed for each of the candidate models. Any models for which the correlation fell within the range of the 95% confidence intervals of the observations were deemed to capture the relationship between the IOD and extreme precipitation in this region sufficiently well to be evaluated further.

Figure 7 shows a violinplot of the correlations in each group of models tested - HighResMIP, CMIP6 and CORDEX - along with the range of values covered by the 95% confidence intervals estimated from the observations. None of the CORDEX models capture the relationship between the IOD and extreme precipitation in this region (see eg. Enris et al., 2015), so these models are not considered further.

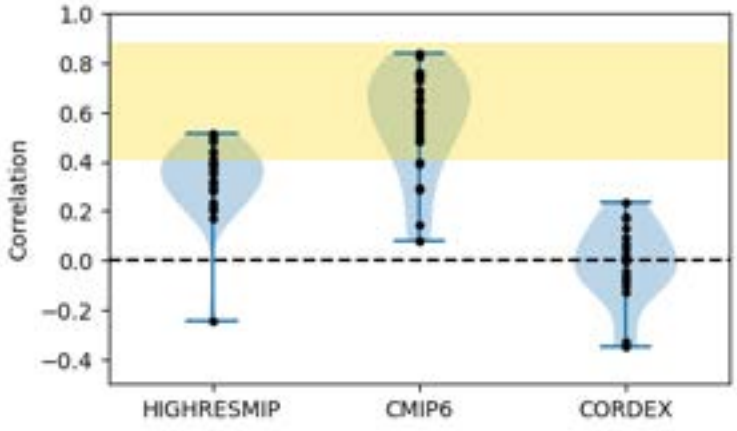

Figure 9: *Violinplots of correlations between model IOD and RX30day in each of the models evaluated. The shaded region shows the range of values covered by the 95% confidence intervals in the observational datasets.*

Those climate models that do correctly represent this relationship were further evaluated for their ability to capture the observed distribution of RX30day, and discarded if the ranges of the key parameters of the fitted non-stationary distribution did not overlap with those estimated from the observations. The models are labelled as ‘good’, ‘reasonable’, or ‘bad’ for both the dispersion and shape parameters, and finally evaluated in terms of how well they represent the spatial and seasonal patterns of precipitation. If the

model is ‘good’ for all criteria, we give it an overall rating of ‘good’. We rate the model as ‘reasonable’ or ‘bad’ overall, if it is rated ‘reasonable’ or ‘bad’, respectively, for at least one criterion. Because so few models achieved a ‘good’ evaluation overall, we also include models deemed ‘reasonable’ in the attribution analysis. Table 1 shows the model evaluation results for those models included in the full study.

Table 1: *Results of evaluation for those models that received an overall rating of ‘good’ or ‘reasonable’. For each model, the best estimate of the scale parameters is shown, along with a 95% confidence interval for each, obtained via bootstrapping. The qualitative evaluation is shown in the right-hand column.*

Model / Observations	**Seasonal cycle**	**Spatial pattern**	**Dispersion**	**Shape parameter**	**Conclusion**
MSWEP			0.291 (0.291 ... 0.291)	-0.017 (-0.49 ... 0.31)	
TAMSAT			0.386 (0.386 ... 0.386)	-0.052 (-0.46 ... 0.21)	
CPC			0.343 (0.261 ... 0.409)	-0.023 (-0.55 ... 0.27)	
HadGEM3-GC31-HM (1)	good	reasonable	0.231 (0.187 ... 0.262)	-0.023 (-0.32 ... 0.20)	reasonable
CMCC-CM2-SR5 (1)	reasonable	good	0.315 (0.267 ... 0.350)	-0.25 (-0.38 ... -0.12)	reasonable
CMCC-ESM2 (1)	reasonable	good	0.278 (0.235 ... 0.315)	-0.092 (-0.31 ... 0.018)	reasonable
GFDL-CM4 (1)	reasonable	reasonable	0.268 (0.226 ... 0.305)	-0.24 (-0.34 ... -0.14)	reasonable
GFDL-ESM4 (1)	reasonable	reasonable	0.267 (0.215 ... 0.307)	-0.18 (-0.32 ... -0.040)	reasonable
NorESM2-MM (1)	good	good	0.375 (0.344 ... 0.428)	0.0024 (-0.16 ... 0.11)	good

5 Multi-method multi-model attribution

Table 2 shows the changes in intensity (ΔI) estimated from each observational dataset and for those models that passed evaluation.

Table 2: *Change in relative intensity of RX30day due to changing GMST: (a) from preindustrial climate to the present and (b) from the present to 2C above preindustrial.*

Model / Observations	**Threshold for 40-year return period (mm)**	**(a) % change in intensity after 1.2C**	**(b) % Change in intensity after further 0.8C**
MSWEP	242	87 (34 ... 129)	
TAMSAT	243	128 (49 ... 202)	
CPC	282	71 (14 ... 128)	

HadGEM3-GC31-HM (1)	44	23 (4.7 ... 42)	
CMCC-CM2-SR5 (1)	93	20 (13 ... 26)	20 (13 ... 23)
CMCC-ESM2 (1)	204	22 (16 ... 27)	19 (14 ... 24)
GFDL-CM4 (1)	222	22 (16 ... 34)	20 (12 ... 26)
GFDL-ESM4 (1)	215	30 (18 ... 42)	28 (15 ... 33)
NorESM2-MM (1)	84	37 (30 ... 63)	19 (18 ... 49)

6 Hazard synthesis

For the event definitions described above we evaluate the influence of anthropogenic climate change on the event by calculating the change in intensity using both observations and climate models. Models which do not pass the evaluation tests described in Section 4 are excluded from the analysis. As most of the available models do not exhibit a correlation between the IOD phase and OND rainfall in the study region, the number of models is small, with only five 'reasonable' models and one good model. We present results here only for the effect of GMST on the intensity of the event, although the IOD is also included in the statistical model, as described in Section 2.3.1.

The aim is to synthesise results from models that pass the evaluation along with the observation-based products, to give an overarching attribution statement and assess whether the changes in intensity in the observation due to GMST are caused by human-induced climate change alone. Including the IOD in the statistical model renders the changes in return times highly uncertain and hard to interpret, so we focus on changes in intensity alone. Figure 10 shows the changes in intensity for the observations (blue) and models (red). To combine them into a synthesised assessment, first, a representation error is added in quadrature to the observations, to account for the difference between observation-based datasets that cannot be explained by natural variability. This is shown in these figures as white boxes around the light blue bars. The dark blue bar shows the average over the observation-based products. Next, a term to account for intermodel spread is added in quadrature to the natural variability of the models. This is shown in the figures as white boxes around the light red bars. The dark red bar shows the model average, consisting of a weighted mean using the (uncorrelated) uncertainties due to natural variability. Observation-based products and models are combined into a single result in two ways. Firstly, we neglect common model uncertainties beyond the intermodel spread that is depicted by the model average, and compute the weighted average of models (dark red bar) and observations (dark blue bar): this is indicated by the magenta bar. As, due to common model uncertainties, model uncertainty can be larger than the intermodel spread, secondly, we also show the estimate of an unweighted, direct average of observations (dark red bar) and models (dark blue bar) contributing 50% each, indicated by the white box around the magenta bar in the synthesis figures.

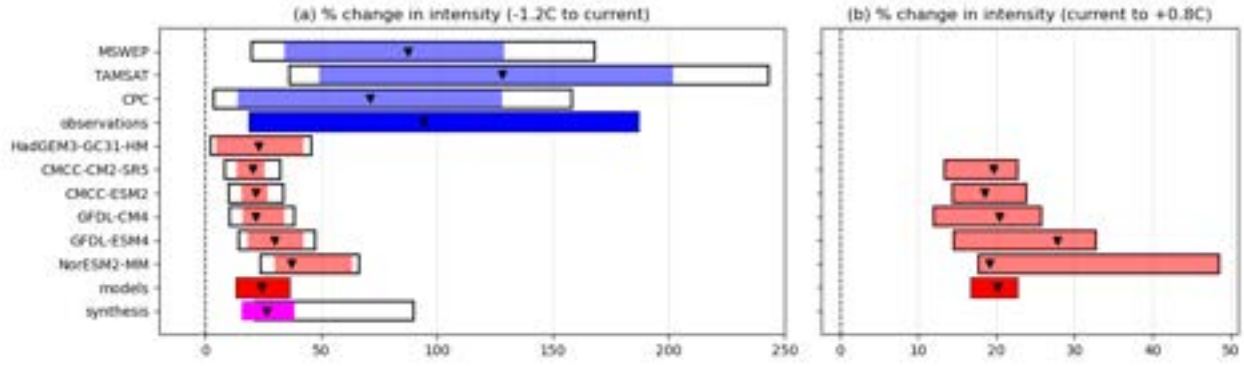

Figure 10: *Synthesis of intensity changes (in %) in RX30day over the study region: (a) comparing the 2023 climate and a 1.2C cooler climate; (b) comparing the current climate and a future 0.8°C warmer climate.*

The six models passing the evaluation tests show a considerably smaller increase in the intensity of RX30-day OND rainfall in the study region than the observations, being largely consistent with the expected Clausius-Clapeyron increase of about 10% with current warming levels. The large increase in intensity due to the increase in GMST of 1.2C in the observations cannot be explained by the warming alone. Thus, unless there is an alternative explanation for the strong trend in observations, the models presumably do not represent a change in the dynamics, e.g. related to the movement of the ITCZ, that explains the additional increase in intensity. All observations-based datasets show an equally strong increase in intensity, and while it is likely that ENSO has some additional effect on the precipitation, it does not vary in the same way as the smoothed GMST used here, so is unlikely to be a strong contributing factor. Given that no other factors changing similarly to GMST are known to have occurred in the region, the model results are presumably conservative. We thus report the upper bound of the unweighted average as the overarching result, stating that human-induced climate change increased the intensity of RX30-day OND rainfall in the study region by up to 100%.

When conducting the same analysis (without the observational data) for a 0.8C warmer world compared to today (fig. 10, right-hand side), we find a similar increase of about 20% as a best estimate with comparably small uncertainty bounds. Due to the large discrepancy between the observations and models we have little confidence in the quantitative change in intensity in the future, but high confidence that future warming will further increase the intensity of OND-rainfall in the Horn of Africa.

Combining all lines of evidence we have very high confidence that human-induced climate change as well as the positive phase of the IOD increased the magnitude of heavy rainfall in heavy OND-rainfall in the study region and that future warming will further increase the intensity. Due to the comparably short time series, especially with respect to positive IOD years and the discrepancy between the models and observations that need further research to explain, the confidence in the exact quantification of the increase is low.

7. Vulnerability & Exposure

Following three severe droughts in the last 12 years, the Horn of Africa (HoA) is currently facing extensive flooding and what climate scientists are calling an “unprecedented disaster” (FAO, 2023). Both of these events indicate the myriad ways in which hazards can result in extraordinary impacts for populations and the environment. While the impact of distinct hazards is important, they should also be seen through the lens of vulnerability and exposure (V&E) factors (IPCC AR6). Understanding the V&E context in which hazards occur can support more thorough assessments of why impacts occurred and

how to avoid or reduce these impacts in the future especially as climate and extreme weather events are forecasted to continue in frequency and severity in the future. This section examines the V&E factors of the recent floods in Somalia, Kenya, and Ethiopia to advance this understanding and contextualisation of this hazard.

7.1 Intersecting vulnerabilities

While communities of the HoA region are no strangers to weather and climate extremes, an increasing number of people lack access to basic services pertaining to water and sanitation, electricity, health, early warning, response, and social protection systems, rendering them highly vulnerable to meteorological shocks (UNDP, 2022; Prieto-Garcia et al., 2022; OHCHR, 2020).

Natural hazards including extreme rainfall and drought are increasing in frequency and intensity in the region (see our WWA study on the 2020-2022 HoA drought, Kimutai et al., 2023), compounding impacts and placing persons engaged in weather-dependent livelihoods in an especially disadvantaged position (Weingärtner et al., 2022; Thalheimer et al., 2023). A poverty trap is created as limited assets prevent people from adequately bouncing back from economic disruptions, damages, and losses (Sherwood, 2013). Beyond pastoralists, this includes elderly people (elderly women in particular) and the poorest in the community (Omolo & Mafongoya, 2019). In this context, flooding is known to increase the cost of living in Kenya, Somalia, and Ethiopia including through rising food prices, which further exacerbates the economic strain on these communities (Weingärtner et al., 2022; Action Against Hunger, 2023; World Vision, 2023; OCHA, 2023). In Kenya for example, household income, size of household, and housing type are key determinants to vulnerability to floods (Odero & Mahiri, 2022). In Somalia, after a series of flood events in 2020 that displaced an estimated 918,00 people (UNHCR, 2023) at the onset of the COVID-19 pandemic, populations have been experiencing intersecting risks and vulnerabilities resulting in dire food security levels (Thalheimer et al., 2023).

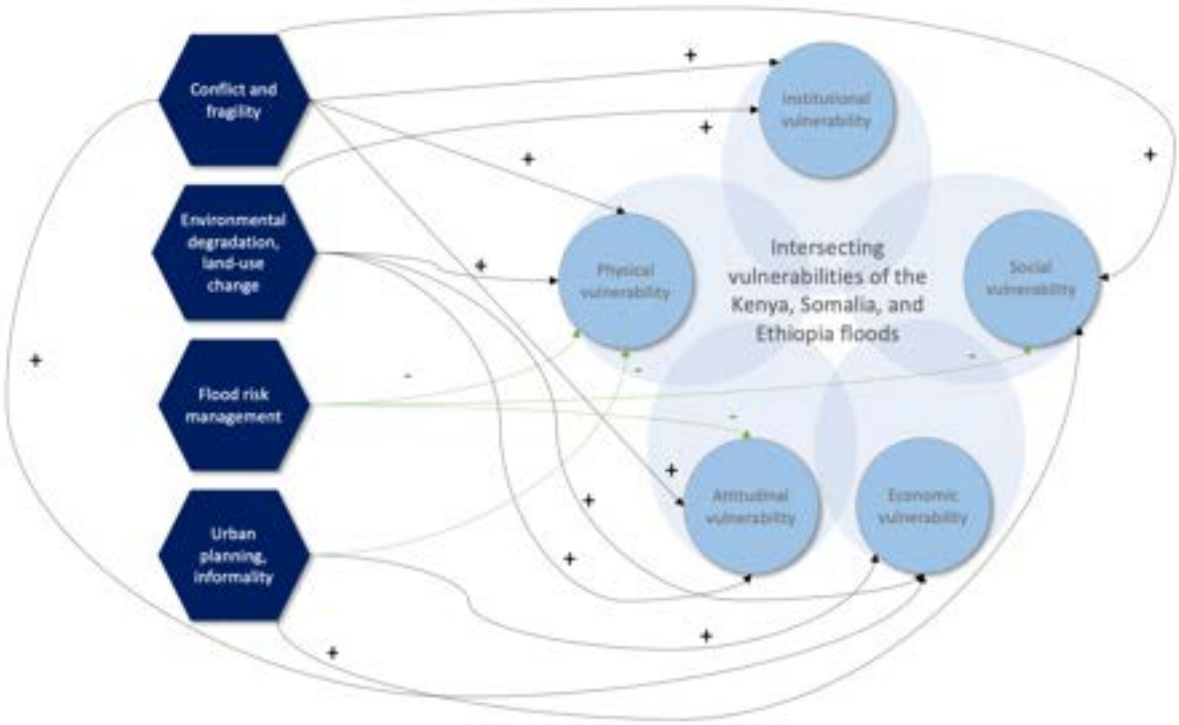

Figure 11: Landscape of flood-related themes showing the influences on five types of vulnerabilities. Arrows indicate root drivers of vulnerability (blue circles) with '-' indicating a mitigating influence on vulnerability type and '+' an aggravating influence.

7.2 Land use land cover changes

Since 1970, significant land use land cover (LULC) changes across the HoA region have aggravated the interlinked risks of both flooding and drought (Prieto-Garcia et al., 2022; Warsame & Sarkodie, 2022). Deforestation and associated soil erosion, urbanization, and unsustainable land management practices including overexploitation of grazing land decrease the water-retention capacity of the land, and in turn increase communities' exposure to extreme rainfall and ensuing floods (Hamud et al., 2021; Barasa & Perera, 2018; Prieto-Garcia et al., 2022; Beshir & Song, 2021; Erena & Worku, 2019). Said changes have also exacerbated the risk of landslides, known to be highly deadly across the three countries (see e.g. OCHA, 2019; OCHA, 2018), including this rainy season.

Between 2002 - 2022, forest land declined by 14% on average across Kenya (Global Forest Watch, 2022a). Sub-nationally, this figure can be substantially higher, such as in the town of Narok where it exceeds 39% (Umukiza et al., 2021). Research by Mireille et al. (2019) suggests that the basic infiltration rate of forest land (89.1 cm/h) is nearly sixfold that of agricultural land (15 cm/h), and more than eleven times that of rangeland (7.9 cm/h). The vast loss of tree cover and associated increase in surface runoff have driven the observed peak river discharge to increase from 167 m3/sec to 233 m3/sec, increasing the risk of flooding and river bank erosion (Barasa & Perera, 2018). In Ethiopia and Somalia, deforestation

rates between 2001 and 2022 reach 18% and 5.1%, respectively (Global Forest Watch, 2022b; Global Forest Watch, 2022c).

Despite repeated attempts to ban firewood and charcoal exports in Somalia, such as in 1969, 2012, and 2016, unrestricted production spiked after the government collapse in 1991, and the charcoal industry continues to constitute a driver of tension and intercommunal conflict (UNEP, 2022). Charcoal and firewood moreover remain the main energy sources in rural and urban areas alike (The Federal Republic of Somalia, 2022). Programmes such as PROSCAL, a joint initiative between UNEP, UNDP, and FAO, is raising awareness on the impacts of illegal charcoal production among people whose livelihoods are threatened by deforestation and supporting them in securing more sustainable jobs (UNEP, 2022). The government of Somalia has also developed a National Environment Policy, meant to promote the country's commitment to environmental conservation and sustainable land-use management in the face of extensive degradation (The Federal Republic of Somalia, 2019).

To restore degraded lands, improve the forestry sector's contribution to food production systems, and create more employment opportunities, the Ethiopian government is aiming to restore more than 20 million hectares of forest and degraded lands by 2023 (Evans, 2018). This includes rehabilitating, conserving and protecting existing forests, and enlisting smallholder farmers to cash and/or food for work programmes. The commitment is embedded in the 2018 National Forest Law, and led by the Ministry of Environment, Forest and Climate Change established ten years ago (Evans, 2018).

In Kenya, a logging ban was introduced in 2018 and remains in place despite recent attempts by the government to lift it to create jobs (Natural Justice, 2023). Rooted in its Reducing Emissions from Deforestation and Forest Degradation (REDD+) strategy, launched in 2020, the government of Kenya is committed to planting over 5 million trees and restoring 5.1 million hectares of forest land, along with achieving an overall 10% tree cover (Republic of Kenya, 2020).

7.3 Urban Planning and Informality

The *State of Africa Cities* report highlights that Eastern Africa is the world's least urbanized sub-region, but it has the fastest rate of urbanization. However, it is projected that by the end of 2040 urbanization will increase rapidly resulting in five times the urban population than that of 2010. The consequences of this unplanned rapid growth in major Eastern African cities include severe housing shortages, traffic congestion, pollution, and unregulated expansion into marginalized, hazard prone land and peri-urban areas (UN Habitat, 2014). The increasing urban population is particularly susceptible to the effects of natural disasters, with flooding being a significant concern in relation to climate change (Jean-Baptiste et al., 2013).

Kenya, particularly in Nairobi with its significant informal settlements, grapples with the aftermath of floods due to inadequate policies considering climate impacts on critical infrastructure (Njogu, 2021). Approximately 60% of Nairobi's population resides in approximately 40 slum neighbourhoods like Kibera and Mukuru Kwa Ruben (Faye, 2023). It has been estimated that Kibera is accommodating around 1 million people, with 5% living within 30 metres of water bodies, thereby increasing vulnerability to

floods (UNFCCC, 2023). Poor waste management and sanitation practices in Kibera also exacerbate urban flooding risk, as evidenced by a 2015 extreme rainfall event affecting over 50% of residents (Galvin & Maassen, 2021). Weak infrastructure also plays a role in making flooding more likely e.g., in the Mukuru Kwa Ruben informal settlement where a lack of effective structural and non-structural measures - rather than heavy rainfall - caused the flooding (Muhatiah, 2021). However, the government has established several measures to address these risks including the Kenya Informal Settlements Improvement project in 2011 with support of the World Bank, the Swedish International Development Cooperation Agency (SIDA) and the Agence Française de Dévelopement (AFD) in 15 urban areas, including Nairobi and Mombasa (Engineering for Change, n.d.; Ministry of Land, PublicWorks, Housing and Urban Development, n.d.). The project aims to enhance the living conditions of people in urban slums by upgrading infrastructure, which includes improving water, waste and sanitation facilities, ensuring tenure security, and engaging in neighborhood planning through collaboration with local communities (World Bank Group, 2011).

Somalia faces increasing climate change impacts, with 12 droughts and 18 floods since 1990, triple the occurrences between 1970 and 1990 (World Bank, 2020). The country is highly susceptible to flash floods during the Deyr and Gu rainy seasons (UNEP-DHI, 2022; UN OCHA, 2021). A government assessment for 2019 floods revealed $260 million in damages, necessitating $350 million for recovery (World Bank, 2020). Over the next five years, potential flooding poses a projected economic damage of up to $206 million to critical infrastructure (World Bank, 2020). The effectiveness and benefits of proposed government solutions such as the National Water Resource Strategy 2021-2025 and technical support from UN agencies towards flash flood risk assessment and researching the applicability of Nature-based solutions for flood and drought mitigation remain to be seen as they are implemented (Federal Government of Somalia, Ministry of Energy and Water Resources, 2021; UNEP-DHI, 2022).

Recently, Ethiopia, especially its capital, has grappled with varying degrees of flooding (Birhanu et al., 2016). Due to conflict in the Tigray region that began in November 2020, two refugee camps in the region hosting Eritrean refugees were completely destroyed, leading the refugees to mainly relocate to Addis Ababa (UNHCR, 2022). As of July 2023, over 930,000 refugees and asylum seekers, mainly in informal settlements in Addis Ababa, face inadequate infrastructure compounded by climate change and deficient urban environmental policies (UNHCR, 2023). The mountainous terrain, degraded by deforestation and soil erosion from informal settlements, lacks proper drainage, waste disposal, and green spaces, heightening vulnerability to shocks and stressors such as flooding (Resilient Cities Network, 2020). Rapid urbanization and informal settlement expansion have ultimately increased the city's overall susceptibility to flooding (Beshir & Song, 2021).

7.4 Conflict and Fragility

In The Horn of Africa, there is longstanding evidence of a connection between socio-economic and political drivers with conflict and fragility (Owain et al, 2018). However, the increased frequency and intensity of climate and extreme weather events is calling sustained attention to the ways in which a changing climate is also linked as a threat multiplier to various forms of conflict, intercommunal tension, violence, and fragility in the region (Kimutai et al, 2023; Meier et al., 2007; von Uexkull et al., 2016). While empirical studies of climate change impacts such as drought, water insecurity, and recurring wet seasons suggest indirect links between climate change and conflict, there remain many analytical

challenges in detecting and attributing these links (Buhaug et al, 2023; Thalheimer et al, 2023). This is not in the least because of the complexity of the dynamics of conflict and variations in the presence of weather and climate-related events across countries in the HoA region (Thulstrup et al., 2020; Thalheimer et al., 2021). Ultimately, the dynamics of climate, conflict, and fragility on the ground are complex and nuanced across contexts. The floods induced by the ongoing Indian Ocean Dipole (Indian Niño) in parts of Ethiopia, Kenya, and Somalia bring these complexities to the fore (CARE, 2023).

In Ethiopia, the unprecedented flooding comes at the same time as the country attempts to respond to the seemingly intractable challenges related to intercommunal violence, disease outbreaks, conflicts, and climate change (UNFPA, 2023). These challenges include the recent drought – which lasted fully three years - as well as the rise and spread of contagion in the form of cholera and civil conflict in Tigray – the country's northernmost region – which first came to international attention in November 2020 (Global Conflict Tracker, 2023; Save the Children, 2023). These combined challenges increase community-level vulnerability and exposure to the impacts of severe flooding including through exacerbating insecurity, dislocation from livelihoods and public services which INGOs have long counted as key components of the country's post-conflict transition (Geda & Degefe, 2005; IMF, 2023; Carnegie Endowment for International Peace, 2023).

In Kenya, conflict-fueled displacement has already led to the world's highest number of refugees, increased patterns of migration and internal displacement. In this context, flooding has dislocated refugees and internally displaced communities from crucial humanitarian assistance while exacerbating loss of livelihoods, destruction of property, and infrastructure damage as refugees struggle to draw on adaptation options due to challenges in continuing registration protocols, health risks related to water and sanitation, and increased mortality rates as the death toll reached 90 people at the end of November 2023 (CARE, 2023). These outcomes exacerbate and compound existing structural and systemic challenges influenced by the recent drought in the region which can potentially overwhelm already scarce response capacities of local and regional humanitarian, development, and community based organizations (UNHCR, 2023; CARE, 2023). In 2022, the UNHCR reported receiving only half of the required USD 137 million in financial resources to respond to the drought in the region compared to the USD 150 million which Education Cannot Wait (ECW) is aiming to raise in response to the 2023 floods in the region (UNHCR, 2023; ECW, 2023).

Several studies suggest that Somalia continues to face one of the most complex challenges of any country in the world since the state collapsed over 30 years ago (Thulstrup et al., 2020). The combined impacts of civil war, the presence of non-state armed groups (such as al-Shabaab) and climate and extreme weather events hamper ambitious efforts towards state building and peace. The International Committee of the Red Cross (ICRC) estimates that hundreds of thousands have been displaced by flooding in conflict affected areas of the country including Beledweyne, Jubaland, Duulow, and Luuq (ICRC, 2023). The floods present new risks to protection and stability in the country as greater numbers experience loss of family links, exposure to water and sanitation challenges, and dislocation from community and social infrastructure (ibid, 2023).

Together, the impacts of flooding in Ethiopia, Kenya, and Somalia demonstrate the complex and nuanced relationship between climate, conflict, and fragility in the HoA. Importantly, they present key lessons for

our understanding of the different ways in which extreme weather events compound risks in contexts of existing instability and conflict.

7.5 Flood Risk Management - A better prepared Horn of Africa

7.5.1 Early Warning Early Action

In July, over three months ahead of the onset of the recent deadly flooding, the Intergovernmental Authority on Development (IGAD)'s Climate Prediction and Application Centre (ICPAC) forecasted the unusually heavy rainfall linked to the ongoing El Niño and positive Indian Ocean Dipole (IOD) (ICPAC, 2023) - as did scientists with the Climate Hazards Center and Famine Early Warning Systems Network (FEWS Net) (Funk et al., 2023). In the following month, the Kenya Meteorological Department (KMD) also forecasted abnormally high seasonal rainfall between October and December (Anticipation Hub, 2023). Again in October, FEWS Net (2023) issued an alert for the projected floods and their expected impacts on agriculture, water and sanitation, transportation, and the economy.

Over the past five years, Somalia has made strides in rebuilding its early warning system for hydrometeorological hazards through a number of projects, including improving monitoring and forecasting weather, climate, and impacts, as well as disseminating early warning and climate information to stakeholder at national to local level (Government of Somalia, 2022). Currently, Somalia has four stations monitoring hydrometeorological conditions, and lacks a centralized and systematic Early Warning System (Federal Government of Somalia Ministry of Energy and Water Resource, 2021). While Somalia, to date, only has a formal mechanism for anticipatory action in place for drought, the country has also developed a Shock Responsive Pilot for early actions (WFP, 2020). Moreover, agropastoralist and pastoralist communities in the country are known to leverage community networks to disseminate early warnings and roll out early actions in anticipation of a number of natural hazards including floods (SPARC, 2022).

In Kenya, the KMD's National Flood Forecasting and Early Warning Centre (NFFEWC) monitors, forecasts, and provides early warnings for floods, targeting disaster risk agencies at national and county levels as well as humanitarian organizations (Kiptum et al., 2023). In Ethiopia, the Early Warning and Response System sits at the National Disaster Risk Management Commission (NDRMC), established in 2016 (REAP, n.d.). To support the translation from an early warning into anticipatory action ahead of the predicted flood onset, the Kenya Red Cross Society (KRCS) and Ethiopia Red Cross Society (ERCS) have each developed an Early Action Protocol (EAP) for riverine floods (Anticipation Hub, n.d.-a; Anticipation Hub, n.d.-b).

Approved in October 2021 and activated on 10 November 2023, after closely monitoring the river levels since early October, the Kenya Red Cross Society (KRCS)'s Early Action Protocol (EAP) for riverine flooding enabled the roll-out of anticipatory action across several sectors, namely shelter, livelihoods and basic needs, health, disaster risk reduction, and water, sanitation and hygiene (WaSH) (Anticipation Hub, 2023). This included handing out cash grants, distributing non-food items and water-treatment chemicals, deploying emergency water-treatment plants, and activating mobile health teams (IFRC, 2023a).

After-action reviews will prove valuable in determining whether and to what extent the early actions were effective in reducing impacts.

The Ethiopia Red Cross Society (ERCS)'s EAP for riverine floods was approved in March 2021 (IFRC, 2021). While focused on the same sectors as outlined above, ERCS's choice of early actions differ, and instead include evacuation of vulnerable populations and livestock, clearing and maintaining drainage channels from agricultural lands, sandbagging around private households, and treating drinking water to prevent contamination (IFRC, 2021). Said EAP was not activated for these floods.

To harmonize the existing anticipatory action initiatives and mechanisms across the HoA, IGAD (2023) has launched the Regional Roadmap for Anticipatory Action (IRRAA). Based on four pillars, its vision includes improving EWS and tools for decision-making for anticipatory action; integrating early action principles into policies across national and regional levels; developing a strategy for the mobilization of resources and partnerships; and strengthening IGAD's coordination role in co-developing and co-implementing anticipatory action at national and sub-national levels.

7.5.2 Social protection

There is a growing interest in studying how social protection systems can be utilized to assist households and communities in dealing with the effects of climate shocks (Costella et al., 2017). Social protection includes various policy tools such as social assistance, social insurance, and labor market policies which can increase the benefits, duration, and number of beneficiaries in existing programs (horizontal expansion), and utilizing the administrative framework for aid delivery during shocks (piggybacking) (ILO, 2022; Oxford Policy Management, 2017). Studies indicate that social protection interventions have an impact on boosting financial and social capital (Khan & Arefin, 2013) and hence play a significant role in enhancing coping strategies for managing floods in particular (Fitrinitia & Matsuyuki, 2022).

In Kenya, social protection is broad based. The National Safety Net Programme of 2013 provides a common operating framework for cash transfer programs such as the Hunger Safety Net Programme (HSNP), the Older Persons Cash Transfer (OPCT) program, Cash Transfers for Orphans and Vulnerable Children (CT-OVC), and the Persons with Severe Disability Cash Transfer (PWSD-CT) program (Republic of Kenya, n.d.). One distinctive aspect of HSNP is its shock-responsive cash transfer system, meaning it can extend its coverage during periods of drought or flooding. This involves providing emergency cash transfers to additional vulnerable households beyond the regular recipients (HSNP, n.d.). In total, these programs benefit over 500,000 households with regular cash transfers. The programs can be expanded in extreme weather events, with approximately 374,806 households in northern Kenya currently receiving cash assistance during such circumstances (Republic of Kenya, n.d.).

Like Kenya, Ethiopia has a primary safety net initiative, the Productive Safety Net Program, launched in 2005 and is currently in its fifth phase. This program, supported by donors, aims to offer a safety net to households facing chronic food insecurity and poverty, often impacted by various shocks (International Food Policy Research Institute, 2014). The assistance is provided through public work programs or, if labor is not feasible, through unconditional support to eligible households. An assessment by IFPRI revealed that over 7 million households belonging to the country's most impoverished individuals

experienced improvements in household food security and the accumulation of assets (International Food Policy Research Institute, 2014).

Somalia, like Kenya and Ethiopia, has a project called Shock Responsive Safety Net for Human Capital (SNHCP). SNHCP offers cash transfers linked to nutrition to help poor and vulnerable households address their immediate consumption needs and guard against the risks of food insecurity and malnutrition (World Bank, n.d.). The project has benefited approximately 1.2 million individuals throughout Somalia (Baxnaano - National Safety Net Programme, n.d.).

V&E Conclusions

Vulnerability and exposure analysis are vital for understanding and assessing hazards in their full context. In parts of Ethiopia, Kenya, and Somalia the flooding has demonstrated how underlying vulnerability and patterns of exposure can lead to differentiated impacts for populations and population sub-groups including refugee, internally displaced, minority ethnic, and other marginalized groups while creating further strictures in the operational response capacity of those government, development, and humanitarian actors attempting to respond to these risks. The recent flooding in the Horn of Africa exemplifies how this underlying vulnerability - exacerbated by unsustainable processes, policies, and systems in environmental degradation and land use, urban planning and informality, disaster risk management, conflict and fragility amongst other factors - increases the scale of flood impacts at the community level. At the same time, this is a nuanced discussion as other elements, such as strong social protection systems and policies to reverse negative trends may help to lessen impacts that could have been worse. As climate and extreme weather events increase in frequency and severity, the HoA flood events also indicate the need for climate-sensitive infrastructure and critical infrastructure including public services and social and communal networks; integration of the compound and cascading risks of mass displacement, various forms of conflict, intercommunal tension, violence, and fragility in addition to socio-economic interventions; as well as increasing the adaptive capacity of systems in early warning early action, response, and social protection to advance resilience in the most vulnerable communities and population subgroups who are often the first and hardest hit by these events.

Data availability

All time series used in this study are available via the Climate Explorer.

References

All references are given as hyperlinks in the text.

Appendix

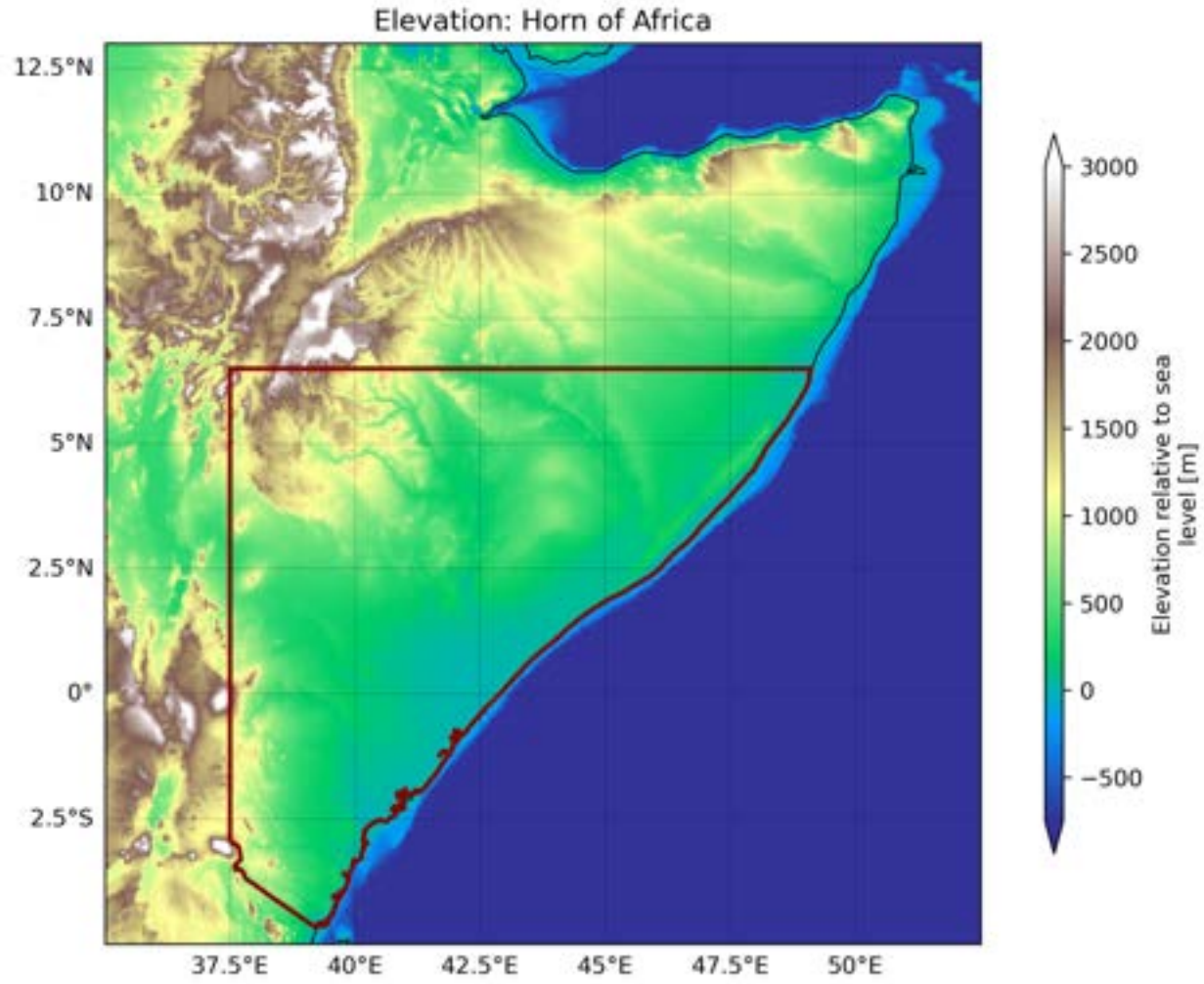

Figure A1: Shows *elevation of Horn of Africa based on [TBASE data] at 0.25° resolution.*

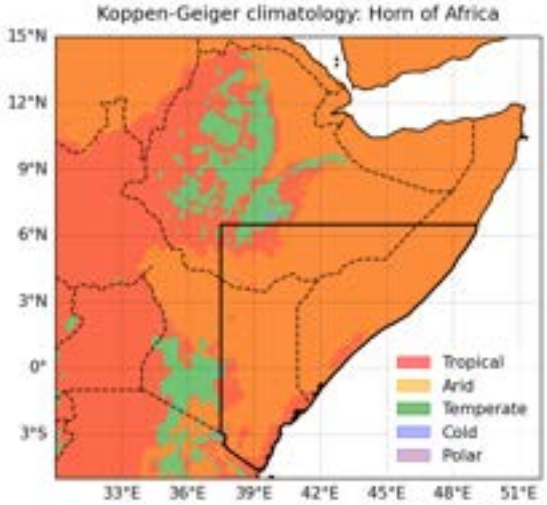

Figure A2:*: Koppen-Geiger climate classification map, using data from [GloH2O].*

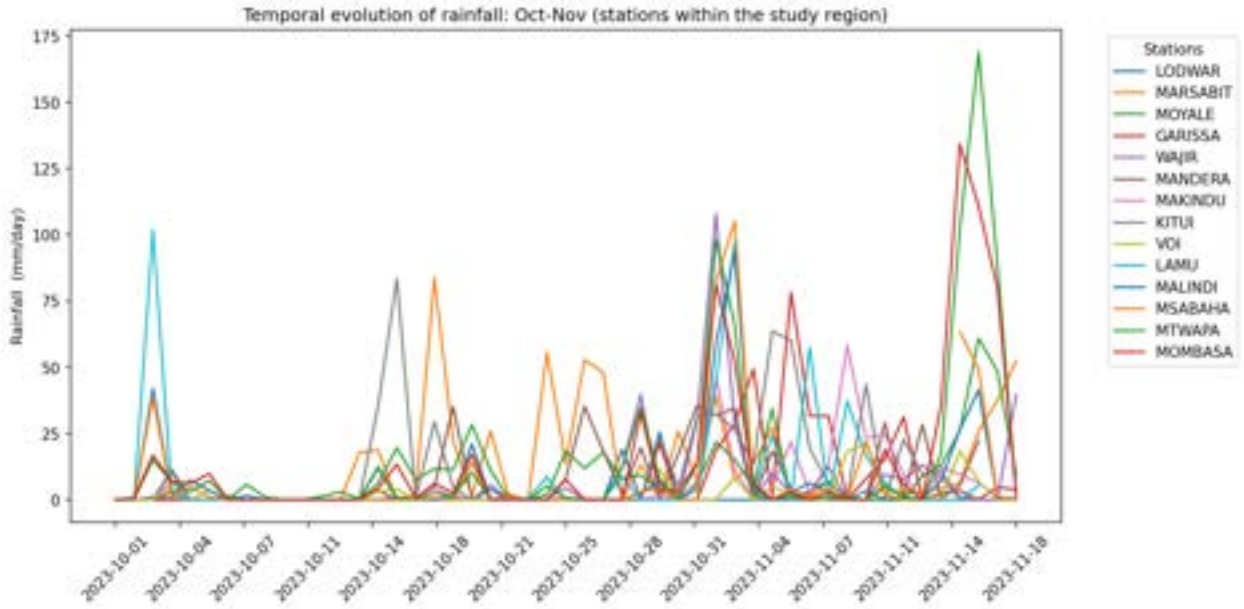

Figure A3: *Daily rainfall in several weather stations in the Kenyan part of the study region. Source: KMD.*

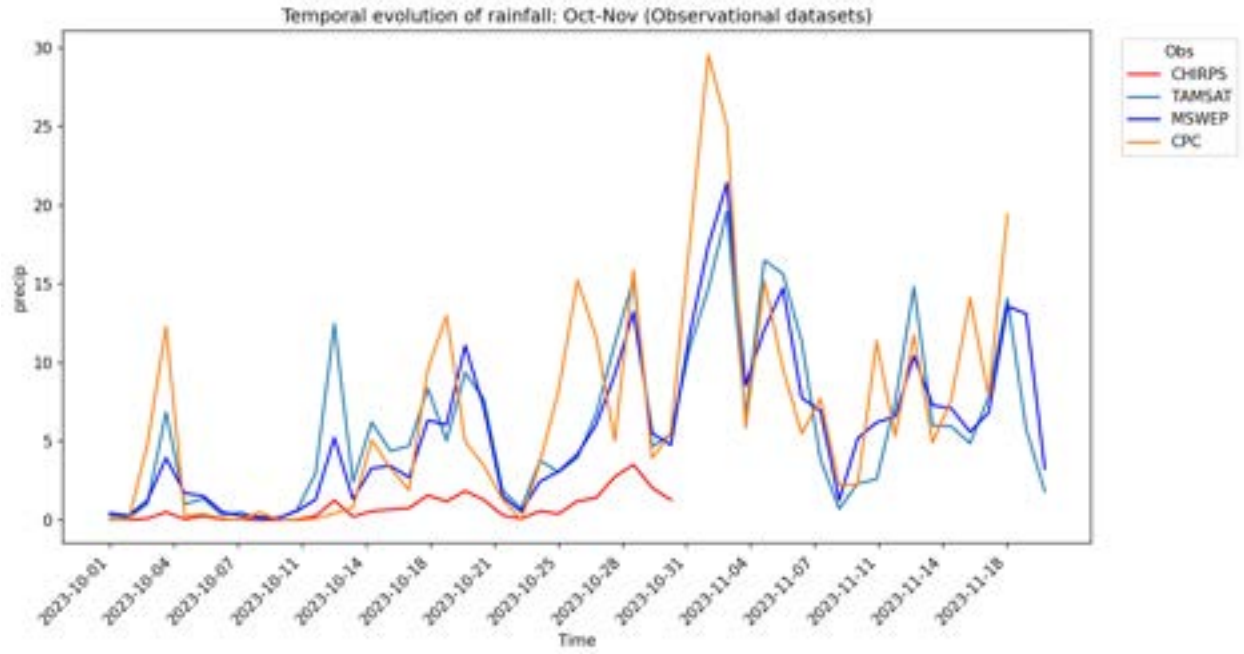

Figure A4: *Daily rainfall in gridded data sets over the study region for October up till the 18th of November 2023.*

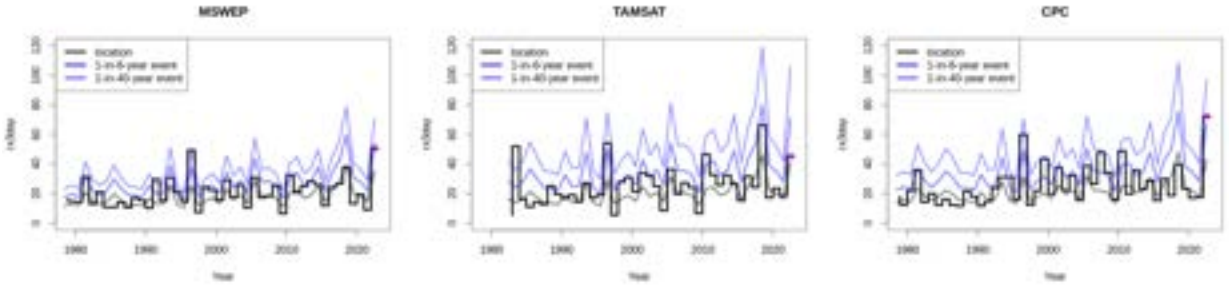

Figure A5: *Time series of RX3day over the study region in the MSWEP, TAMSAT and CPC datasets. The pink dot marks the 2023 event; the heavy black line indicates the location of the fitted distribution, and the blue lines indicate estimated 6- and 40-year return levels.*

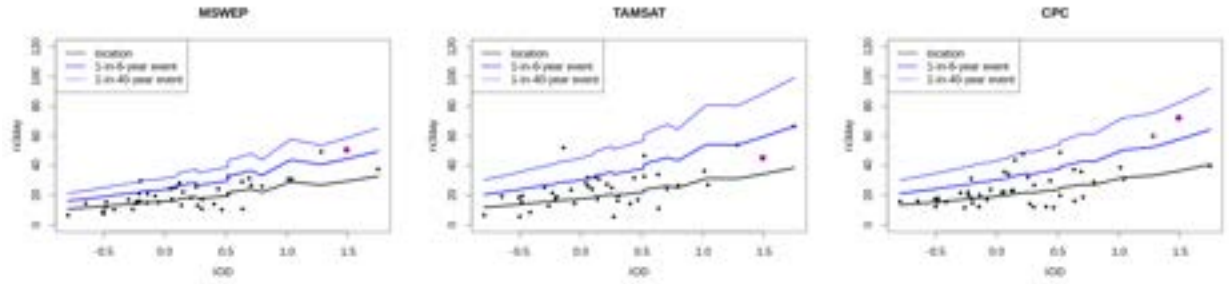

Figure A6: *Observed values of RX3day in the MSWEP, TAMSAT and CPC datasets, plotted against the IOD, with the GMST held fixed at the 2023 level. The pink dot marks the 2023 event; the heavy black line indicates the location of the fitted distribution, and the blue lines indicate estimated 6- and 40-year return levels.*

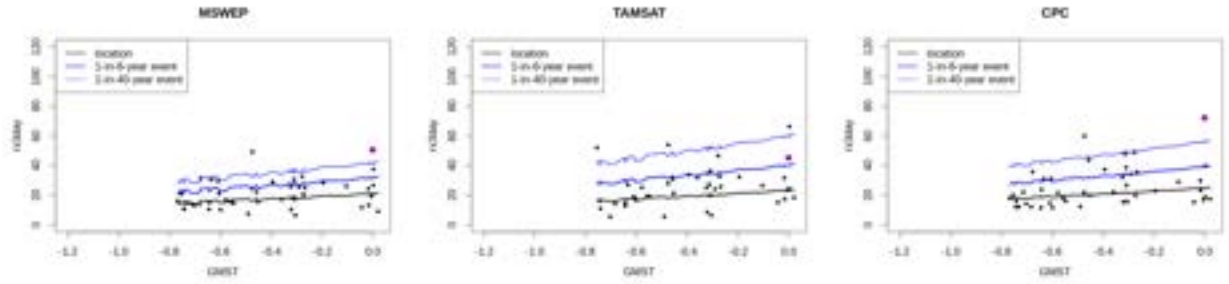

Figure A7: *Observed values of RX3day in the MSWEP, TAMSAT and CPC datasets, plotted against GMST, with the IOD held fixed at 0. The pink dot marks the 2023 event; the heavy black line indicates the location of the fitted distribution, and the blue lines indicate estimated 6- and 40-year return levels.*